Direct observation of Fermi-pressure-driven electron-hole plasma expansion in GaAs on a picosecond time scale

R. Ziebold, T. Witte, M. Hübner, and R. G. Ulbrich
IV. Physikalisches Institut Universität Göttingen, Bunsenstrasse 13/15, D-37073 Göttingen, Germany
(Received 19 November 1999)

Applying pump and probe differential reflection (ΔR) and transmission (ΔT) of femtosecond light pulses for either co- or counterpropagating pump and probe geometries, a direct time of flight method with submicrometer resolution is presented. With this technique we study the density-dependent transport of photogenerated carrier plasmas perpendicular to the surface of GaAs samples for delay times 20 ps$\leqslant\tau\leqslant$1 ns. At a pump fluence of 800 μJ cm^{-2} a relatively sharp charge-carrier front was observed, with high velocities of 14×10^5 cm/s at a delay time $\tau\approx20$ ps, decreasing as $v\propto\tau^{-2/3}$ to 2×10^5 cm/s at $\tau\approx350$ ps. The arrival times τ of the carriers at a fixed sample thickness depend on the fluence of the pump pulses F such as $\tau\propto1/F^{0.45}$. The results are discussed in the framework of diffusive transport with a strongly density-dependent diffusivity D. The data can be described consistently with the assumption of Fermi pressure as the dominating driving force for plasma expansion.

I. INTRODUCTION

Over the last two decades there has been considerable interest in the dynamics of photogenerated carrier plasmas in semiconductors on short length and time scales. The temporal dynamics of spatially homogeneously generated electron-hole pairs in the range of 10 fs–100 ps has been thoroughly studied and is quite well understood.[1] The spatiotemporal dynamics of electron-hole plasmas (EHP's) is less well understood and is still a subject of controversial discussion. The expansion of the plasma has been observed both perpendicular and parallel to the excited surface, with various experimental techniques, such as time and/or spatially resolved luminescence,[2–6] Raman spectroscopy,[7] four-wave mixing,[8–10] laser ultrasonics,[11] and time-of-flight[12–14] (TOF) measurements. For simplicity, only direct semiconductors will be discussed here. We will distinguish between *lateral* expansion with generally smaller density gradients and plasma expansion *perpendicular* to the surface with higher density gradients.[7] This distinction is useful because of the specific influence of the surface on these two transport schemes.

For lateral transport, especially when observed on multiple-quantum-well structures, high diffusivities and carrier-density-dependent diffusivities were found and have been attributed to ballistic phonon wind at low temperatures[14] and screening of impurity scattering.[13] Hillmer *et al.*[3] discussed photon-assisted transport via emission and reabsorption of photons, where the quantum-well structure acts as a waveguide for the photons. Among others[10,4] Fox and van Driel also explained their results on lateral transport for delay times $\tau<10$ ps with this photon recycling mechanism and pointed out that it is not proportional to the carrier-density gradient and hence cannot be described by a diffusion equation.[8]

In direct comparison with lateral transport Tsen *et al.*[7] found a much faster perpendicular transport of carriers in InP at $T=300$ K. To describe their results they introduced phenomenologically an additional drift velocity term in the diffusion equation. Such a drift velocity term was also used by Hillmer *et al.* for their TOF experiments in $Ga_xAl_{1-x}As$.[12] The underlying driving force for the fast plasma expansion perpendicular to the surface has hitherto not been clearly identified. The reason why perpendicular transport is less well understood is that most of the experiments were only sensitive to the temporal evolution of the carrier density on the front side of the sample where they have been generated.[5–7,11] From these measurements direct conclusions on carrier velocities are not possible, because the surface carrier density is not only determined by the carrier transport but also by all kinds of recombination processes, especially by surface recombination.[12] In TOF measurements with a double quantum well acting as a carrier probe, performed by Hillmer *et al.*,[12] the temporal resolution was restricted to >200 ps, limited by the process of carrier capture and the finite lifetime of the quantum-well states.

The TOF technique, described here, enables the observation of initial plasma transport for times <100 ps. In this paper we present carrier-density-dependent TOF studies on GaAs at $T=300$ K with fluences up to 800 μJ cm^{-2}. The results are compared with an isothermal hydrodynamic model with a density-dependent diffusivity, excluding an extra drift term. The density dependence of the diffusivity results from the Fermi pressure, i.e., from the enhancement of the free energy of the charge-carrier system with the onset of degeneracy.

The temporal evolution of carriers generated by ultrashort light pulses can into principle be divided into four different regimes.[1] After the coherent ($\leqslant200$ fs) and the nonthermal regime ($\leqslant2$ ps) the carriers reach the hot-carrier regime, where the carrier distribution function can be described with a quasitemperature T that is different from the lattice temperature T_L. Via carrier-phonon scattering the carriers cool down to the lattice temperature within $\sim1-100$ ps (isothermal regime). Finally the semiconductor reaches thermal equilibrium via different electron-hole recombination pro-

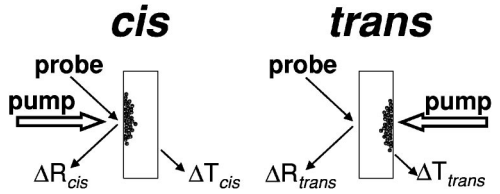

FIG. 1. Pump and probe geometry for the TOF measurement (a) pump front–probe front (*cis*) and (b) pump back–probe front (*trans*).

cesses. In our experiment carrier transport is observed on time scales of the hot carrier and the isothermal regime.

II. EXPERIMENTAL METHODS

In a TOF experiment the fraction N of carriers that have traveled over a given distance d within a time t after starting at $z=0, t=0$ is measured. The knowledge of $N(t,d)$ provides direct access to the transport properties of the carriers under investigation. In our experiment the carriers were generated near the surface of a GaAs sample with variable thickness ($0.8\,\mu\text{m} \leqslant d \leqslant 2.5\,\mu\text{m}$) by laser pulse excitation (pump pulse) with a pulse duration ~ 100 fs. The resulting changes in the dielectric properties of the sample were probed by simultaneously measuring the intensity change of the reflected probe pulses (ΔR) and the intensity change of the transmitted probe pulses (ΔT) as a function of the time delay τ between the pump and probe pulses. Whereas the transmitted probe pulses contain a spatial average over the sample thickness, the ΔR measurement in absorbing samples is mainly sensitive to carriers near the reflecting surface of the sample within a depth given by approximately half of the absorption length $1/\alpha$ of the probe pulses. Changes of the dielectric properties beyond this depth have a negligible influence on ΔR.

The idea of our TOF experiment is simple: We measure $\Delta R(\tau)$ and $\Delta T(\tau)$ first with pumping the front side of the sample (*cis*) and then pumping the back side of the sample (*trans*) (see Fig. 1). The comparison of *cis* and *trans* allows us to draw conclusions about the transport of the initially inhomogeneously distributed carriers.

$\Delta R(\tau)$ and $\Delta T(\tau)$ provide not only different information on the spatial but also on the energetic carrier distribution functions. The dominating contribution to the change of transmission is bleaching due to phase-space filling[1] because of Pauli's exclusion principle, resulting in an increase of transmission if carriers are energetically located in the region of the probed transition. The dependence of ΔR on the energy distribution function of the electrons and holes is more complex. Assuming a thermal distribution function it can be shown that a charge carrier distribution centered above the probed transition energy results in a decrease of reflection and a corresponding carrier distribution centered below the probed transition energy causes an increase in reflection.[15,16] Therefore the sign of ΔR at a given photon energy of the probe pulses provides information about the mean carrier energy. In both ΔR and ΔT the contributions from the electrons and the holes to the signal are additive [$\Delta R; \Delta T \propto (f_e + f_h)$] in contrast, e.g., to the luminescence where the contributions of electrons and holes are multiplicative ($f_e f_h$).

Since the spatial resolution depends on the absorption length of the probe pulses a proper choice of the probe photon energy E_{probe} has to be done. The spatial resolution with a probe photon energy near the band edge E_g of GaAs, where the interband transitions from the heavy hole (hh) and light hole (lh) to the conduction (c) band are probed, is rather poor [$\frac{1}{2}(1/\alpha_{probe}) \sim 0.5\ \mu$m]. A significant enhancement by a factor of 3 can be achieved by using a probe photon energy near the transition from the spin-orbit-split hole (soh) band to the conduction band (see inset of Fig. 4):

$$E_{probe} \approx E_g + \Delta_{soh}$$

with the spin-orbit-splitting energy Δ_{soh}. For sufficiently small E_{pump} the soh band is nearly unoccupied, which means that the main contributions to ΔR and ΔT arise from the electrons in the conduction band. First introduced by Alexendrou *et al.*,[18] a pump-probe technique probing the soh-c transition was applied in a ΔT measurement to separately monitor the electron dynamics and to eliminate the influence of coherence effects to the signal. To the best of our knowledge the soh-c transition has not been used in ΔR measurements. Therefore the applicability of probing the soh-c transition in $\Delta R(\tau)$ measurements has been carefully checked (see Sec. IV). The fact that only the electron dynamics is observed does not influence our method, because we focused our interest on *ambipolar* transport of electrons and holes together.

This TOF method in a standard pump and probe scheme with its high spatial and temporal resolution allows direct observation of rapidly expanding carrier plasmas and should be compared with other capable TOF techniques such as the so-called imaging experiments,[2] where a temporal resolution of $\sim$nanoseconds and a spatial resolution of $\sim$micrometers was reached. Very high spatial resolution has been achieved in experiments where the luminescence of quantum wells with different thicknesses were used as a carrier probes.[12] This technique is restricted to distinct sample thicknesses and is a rather indirect measurement because one has to consider additionally the process of carrier capture and the finite lifetime of the recombining states.

III. EXPERIMENTAL DETAILS

The measurements were made at 300 K on semi-insulating GaAs ($E_g = 1.428$ eV), which was grinded and etched to a minimum thickness of 0.8 μm. The thinning process resulted in a sample with a flat surface on one side and a curved surface on the opposite side, where the effective thickness d, depending on the lateral position of the laser spot, could be varied in the range $0.8\,\mu\text{m} \leqslant d \leqslant 2.5\,\mu\text{m}$.

For our measurements we used an optical parametrical amplifier (OPA) system based on a Ti:sapphire regenerative amplifier which produces (i) ~ 50 fs and full width at half maximum (FWHM) $\sim 5\ \mu$J pulses at a photon energy of 1.5 eV, (ii) a white-light continuum, (iii) frequency-doubled pulses at 3 eV, and (iv) 50 nJ OPA signal pulses tunable from 1.65 eV to 2.75 eV at a repetition rate of 250 kHz. For the minimization of the chirp and for spectral filtering suitable pulse shapers were employed and pulse durations

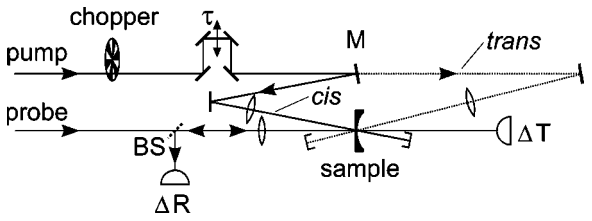

FIG. 2. Experimental setup (M, mirror on a magnetic mount; BS, beam splitter; $\Delta R, \Delta T$, photodiodes).

$\sim$100 fs were reached for all pulses used in our two-color experiments.

The pump beam chopped with a frequency of 700 Hz was focused either on the front or the back side, respectively, of the sample at an incidence angle of 20° and a spot diameter of ≈ 20 μm. The total optical path lengths to the front and back side of the sample were equalized, so that switching between the paths could easily be done with a removable mirror on a magnetic mount (see Fig. 2). After passing a beam splitter ($r/t = 90/10$) the probe beam was focused on the front side of the sample at normal incidence to about 2/3 the spot diameter of the pump beam. The reflected probe beam, collected with the same optics as the incoming beam, was reflected from the beam splitter and collimated, like the transmitted probe beam, to a photodiode. To reduce the influence of laser intensity fluctuations on the measured signals, photodiodes with opposite polarity injected with parts of the probe beam have been used to compensate the signals of the reflected and transmitted probe beam, respectively. In connection with two separate lock-in amplifiers, intensity changes smaller than $10^{-4} I_0$ could be detected. Zero delay between pump and probe was determined with the leading edge of the $\Delta T(\tau)$ signal with an absolute inaccuracy <200 fs and a relative inaccuracy between the two pumping configurations of <50 fs.

The spatial overlap between the pump and probe beam spots was very carefully adjusted with the help of a microscope objective that images the sample on a charge-coupled device (CCD) camera. The sample thickness at each position of the probe beam focus on the sample was determined by precise measurement of the transmission ratio I/I_0 of the probe beam with an extra lock-in amplifier. Together with the known absorption and reflection coefficients[17] of GaAs at the probe photon energy, the thickness was determined. The (systematic) error in the determination of the sample thickness was estimated with the independent measurement of the transmission of the pump beam to be less than 10%. We have specified the fluence F of the pump beam, rather than the initial carrier density n, because of the bigger uncertainty in the determination of n.

IV. RESULTS

A. Comparison of *cis* and *trans* in $\Delta R(\tau)$ and $\Delta T(\tau)$

To demonstrate the applicability of our TOF method, $\Delta R_{cis}(\tau), \Delta T_{cis}(\tau)$ and $\Delta R_{trans}(\tau), \Delta T_{trans}(\tau)$ were measured immediately one after the other (see Fig. 3) at a sample thickness of 2.0 μm. The carriers were injected at a pump photon energy of $E_{pump} = E_g + 470$ meV, resulting in a carrier distribution function with initially high kinetic energies.

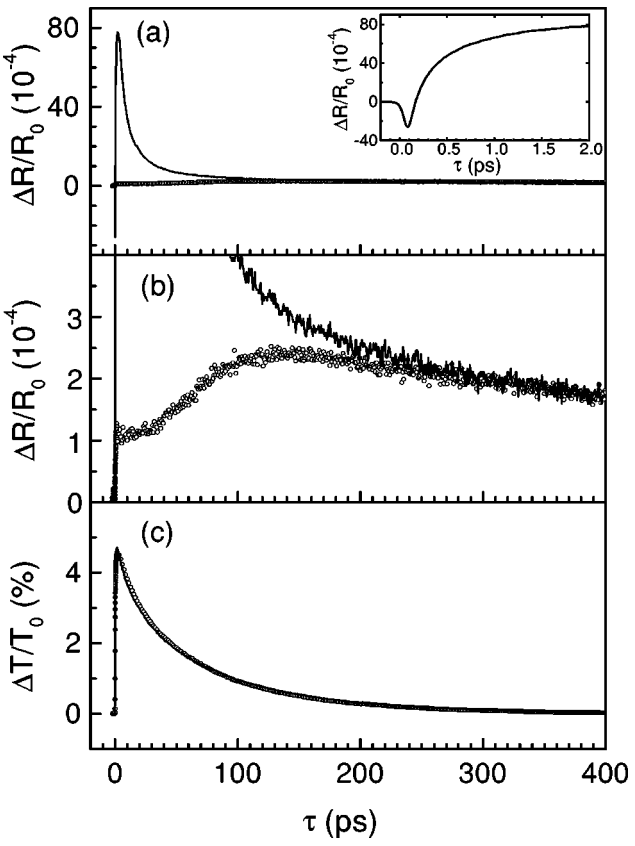

FIG. 3. Comparison of $\Delta R_{cis}(\tau), \Delta T_{cis}(\tau)$ and $\Delta R_{trans}(\tau)$, $\Delta T_{trans}(\tau)$: $E_{pump} = E_g + 470$ meV; $E_{probe} = E_g + 56$ meV; $F = 160$ μJ cm^{-2}. (a) $\Delta R_{cis}(\tau)$ (line) and $\Delta R_{trans}(\tau)$ (open circles). Inset: early times of $\Delta R_{cis}(\tau)$. (b) $\Delta R_{cis}(\tau)$ and $\Delta R_{trans}(\tau)$ with a 20$\times$ magnification. (c) $\Delta T_{cis}(\tau)$ (line) and $\Delta T_{trans}(\tau)$ (open circles).

The absorption length at this energy is $1/\alpha_{pump} = 0.3$ μm. In this experiment the probe photon energy was set to $E_{probe} = E_g + 56$ meV, i.e., only hh-c and lh-c transitions were probed.

After an initial negative peak of $\Delta R_{cis}(\tau)$ with a change in sign at $\tau \approx 200$ fs a maximum is reached at $\tau \approx 3$ ps followed by a decay on a 50 ps time scale. As already mentioned above, the initial negative ΔR arises from a carrier distribution function centered above the probed transition, so that in this particular case the center of the distribution function reaches the energy of $E_{probe} = E_g + 56$ meV already within about 200 fs. This is a fingerprint of a very fast thermalization and cooling down of the carriers.[1] This fast change in $\Delta R(\tau)$ demonstrates also the high temporal resolution of our setup.

In comparison with $\Delta R_{cis}(\tau)$ the temporal evolution of $\Delta R_{trans}(\tau)$ is significantly different. After an instantaneous rise at $\tau = 0$ a slow rise with a maximum at about 150 ps can clearly be identified [see Fig. 3(b)]. After 150 ps the ΔR_{trans} and ΔR_{cis} curves begin to coincide and at 300 ps they are indistinguishable from each other within the experimental error. In principle the ΔR_{trans} signal can be divided into two contributions. The first arises from the carriers that are already generated within the detection volume. This contribution should have a comparable time evolution like ΔR_{cis} and leads to the initially fast rise of ΔR_{trans}. The second contri-

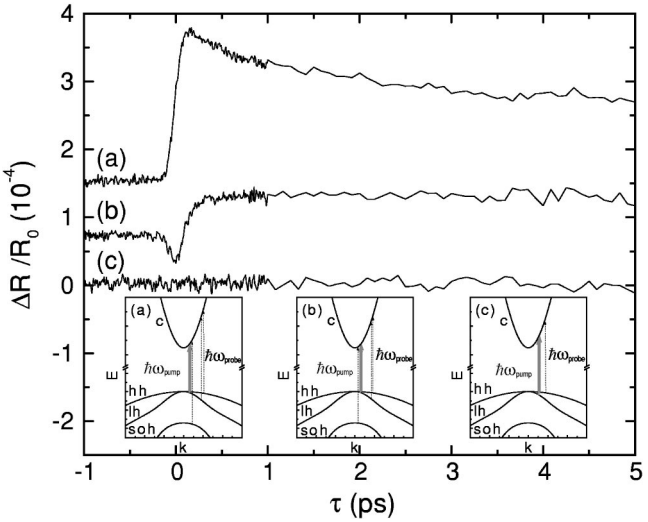

FIG. 4. ΔR_{cis} at variation of E_{probe} around the soh-c transition: (a) $E_{probe}=E_g+\Delta_{soh}+51$ meV; (b) $E_{probe}=E_g+\Delta_{soh}+10$ meV; (c) $E_{probe}=E_g+\Delta_{soh}-90$ meV. In the insets a schematic band structure together with the pumped (solid arrows) and probed transitions (dashed arrows) is displayed.

bution results from carriers that are not generated initially within the probed volume but reach this volume later. The observed maximum at $\tau\approx 150$ ps is undoubtedly caused by this carrier transport. The merging of the ΔR_{cis} and ΔR_{trans} signals after 300 ps can be explained by a spatially homogeneous carrier distribution that is established after this time delay.

As expected the $\Delta T_{cis}(\tau)$ and $\Delta T_{trans}(\tau)$ curves are equal [see Fig. 3(c)], because ΔT includes no spatial information. In fact ΔT curves are independent monitors for the energy relaxation and recombination of the carriers.

B. Differential reflection at the soh-c transition

As mentioned in Sec. II the applicability of probing the soh-c transition in ΔR measurements had to be checked. Therefore we varied E_{probe} around the energy of $E_g+\Delta_{soh}$ while measuring the $\Delta R_{cis}(\tau)$. The spectral resolution was limited by the spectral width of the probe pulses of ~ 16 meV. The carriers were generated near the band edge with $E_{pump}=E_g+100$ meV. For these measurements three representative experimental curves are shown in Fig. 4 together with a schematic picture of the pumped and probed transitions in the insets.

At a probe energy 51 meV above the soh-c transition a relatively large positive ΔR signal is detected [see Fig. 4(a)]. In this case the electrons were generated energetically below the probed transition. In agreement with the expected behavior described in Ref. 16, the experimental curve shows a positive $\Delta R_{cis}(\tau)$.

In curve (b) of Fig. 4, where the electrons were initially generated energetically above the probed transition, the ΔR_{cis} signal consists of a negative part at short time delays around $\tau=0$ and a following positive signal with a slow decay. The fact that there is no signal within the experimental error at E_{probe} below the soh-c transition allows the conclusion that the hh-c and lh-c transitions which are always instantaneously probed, do not provide a significant contribution to the ΔR signal. This fact arises from two reasons. First, there are only very few carriers available for these transitions, and second, because of the higher density of states these carriers cause a comparably smaller band filling and hence a smaller change of the optical constants.

With the experimental results of Fig. 4 we conclude that ΔR measurements with probing the soh-c transition are sensitive to pump-induced carrier populations. All the following experiments were performed with a fixed probe photon energy of $E_{probe}=E_g+\Delta_{soh}+54$ meV where the maximum ΔR signal originating from the soh-c transition was reached.

C. Variation of the sample thickness

After checking the applicability of our method, TOF measurements were performed, to observe the spatiotemporal dynamics of charge carrier plasmas perpendicular to the sample surface. In the following studies the key parameters of our experiments, (i) the sample thickness, (ii) the photon energy, and (iii) the fluence of the exciting laser pulses have been varied systematically.

As a starting point the variation of the sample thickness will be discussed. The carriers were injected at a pump photon energy of $E_{pump}=E_g+1.0$ eV and a resulting absorption length of $1/\alpha_{pump}=0.11$ μm.

An easy interpretation of TOF measurements is only possible if the response time of the detection scheme is shorter than the time constant on which the carrier transport takes place. As a result, the maximum in $\Delta R_{cis}(\tau)$ occurs at shorter time delays τ than the maxima in $\Delta R_{trans}(\tau)$, which can be attributed to the arrival of the carrier front in the detection volume close to the front side of the sample.

A comparison between $\Delta R_{cis}(\tau)$ and $\Delta R_{trans}(\tau)$ at the thinnest observed sample thickness $d=0.8$ μm is shown in the inset of Fig. 5. It clearly demonstrates that the two signal maxima are sufficiently separated in time. Variation of the sample thickness results in drastic changes of $\Delta R_{trans}(\tau)$ (see Fig. 5). The $\Delta R_{trans}(\tau)$ curves at thicknesses $d<1.4$ μm show an instantaneous rise at $\tau=0$, which can be attributed to the initially generated carriers in the detection volume of ΔR_{trans}, as already discussed in Sec. IV A. The decrease in height of this initial ΔR_{trans} signal with increasing sample thickness d supports this interpretation. At sample thicknesses $d\geqslant 1.4$ μm this initial signal is absent and the $\Delta R_{trans}(\tau)$ signal remains zero until a relatively fast rise at later delays τ depending on the thickness d. The delay τ at which $\Delta R_{trans}(\tau)$ is rising corresponds to the time that the carriers need to travel over the distance d through the sample. The relatively short rise times are remarkable, because they indicate that a relatively sharp carrier front is traveling through the sample.

To systemize the quantitative evaluation of the $\Delta R_{trans}(\tau)$ curves in order to obtain the transport properties such as carrier velocities, time delays τ_{HM} were determined, where the $\Delta R_{trans}(\tau)$ signals reach half of their maximum signal. This τ_{HM} is well defined and can be considered as the arrival time of the carriers. In Fig. 6 the thickness d versus τ_{HM} is shown on a linear and a double logarithmic scale (inset), respectively. Figure 6 shows that the carriers travel with initially relatively high velocities ($v\approx 14\times 10^5$ cm/s)

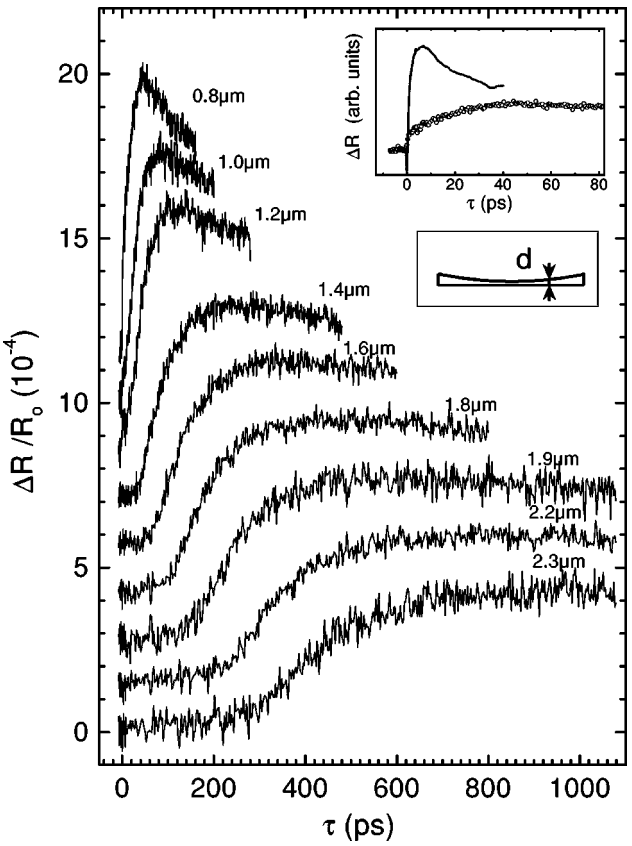

FIG. 5. ΔR_{trans} at variation of the sample thickness d. For clarity a constant offset is added to the $\Delta R_{trans}(\tau)$ curves at different thicknesses d ($E_{probe}=E_g+\Delta_{soh}+54$ meV, $E_{pump}=2.44$ eV, $F=800$ μJ cm^{-2}) In the inset $\Delta R_{cis}(\tau)$ (solid line) is shown together with $\Delta R_{trans}(\tau)$ at $d=0.8$ μm (open circles).

and slow down to velocities in the range of $v\approx 2\times 10^5$ cm/s. In the double logarithmic plot all experimental values are lying on a straight line with a slope of $p=0.33$, so that the correlation between τ_{HM} and sample thickness can be well described by the empirical relation

$$d\propto \tau_{HM}^{p}, \quad p=0.33.$$

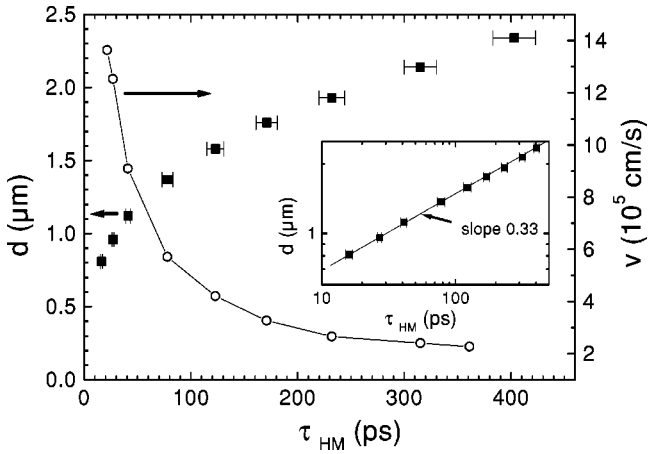

FIG. 6. TOF diagram [corresponding to the $\Delta R_{trans}(\tau)$ curves of Fig. 5] where the sample thickness d (solid squares + left axes) and the resulting velocities (open circles + right axes) are plotted versus τ_{HM}. In the inset the thickness d versus τ_{HM} is shown on a double logarithmic scale.

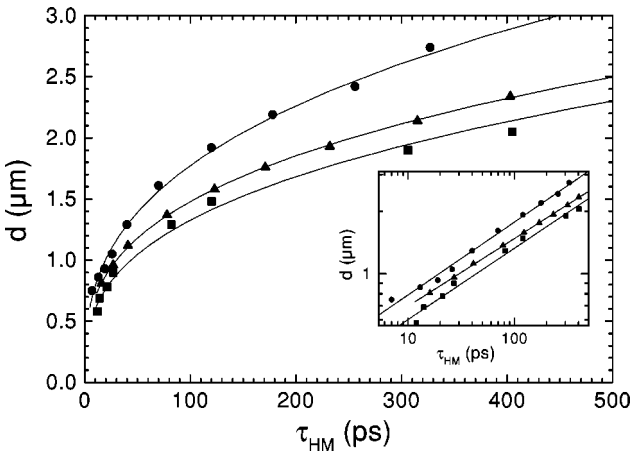

FIG. 7. TOF diagrams for different photon energies of the pump pulses E_{pump} (squares, $E_{pump}=E_g+1.65$ eV; up triangles, $E_{pump}=E_g+1$ eV; circles: $E_{pump}=E_g+0.63$ eV) with the same averaged laser power corresponding to fluence of $F\approx 800$ μJ cm^{-2}.

In comparison, a simple diffusive transport with a constant diffusivity D would lead to a slope $p=0.5$. To the best of our knowledge, this is the first experimental finding that allows a direct comparison with a theory of plasma transport on the reported time and length scales. A rather simple model, describing the experimentally found dependence will be presented in Sec. V.

D. Variation of pump photon energy

To investigate the dependency of the plasma expansion velocity on the initial kinetic energies of the carriers we performed TOF measurements for three different excess energies ΔE of the exciting laser pulses, $\Delta E_{pump}=1.0$ eV, 1.65 eV and 0.63 eV. For these measurements the average laser power at different energies of the pump beam was set to be the same. Again, the sample thickness d is plotted against τ_{HM} (Fig. 7). The results show that the correlation between the sample thickness d and τ_{HM} is qualitatively the same for all three curves. On the first view it is surprising that those carriers, which initially had the lowest kinetic energies, seem to be the fastest. Two reasons could be responsible for this behavior. First, with increasing E_{pump} the absorption length $1/\alpha_{pump}$ decreases, and second, the number of generated electron-hole pairs also decreases if the average laser power is set to be constant. Therefore with increasing E_{pump} the initially generated carriers have, on the one hand, a higher kinetic energy, but on the other hand, less carriers were injected and the latter ones closer to the surface. The actions of these two effects make an easy quantitative interpretation of the measurements difficult.

E. Variation of the fluence of the exciting laser pulses

To study the dependence of the plasma transport on the charge-carrier density, $\Delta R_{trans}(\tau)$ was measured at a fixed sample thickness of $d=1.0$ μm with different averaged laser powers of the pump beam. This was done with a precision variable beam splitter so that all other experimental parameters, especially the lateral position of the pump beam focus on the sample, were unchanged. The very strong dependence of $\Delta R_{trans}(\tau)$ on the pump fluence is shown in Fig. 8. With

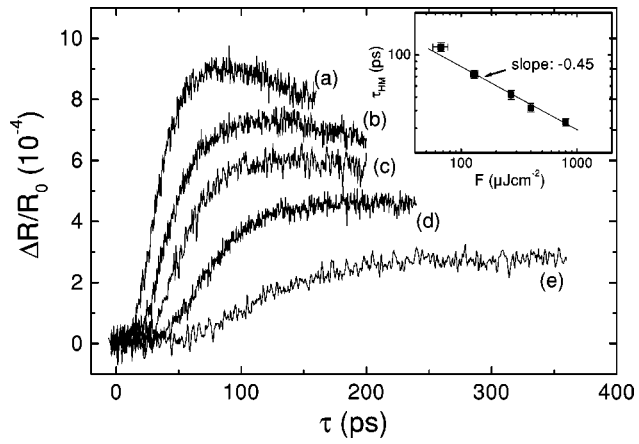

FIG. 8. $\Delta R_{trans}(\tau)$: Variation of the fluence of the pump pulses at a fixed sample thickness of $d=1.0$ μm. (a) $F=800$ μJ cm^{-2}, (b) $F=400$ μJ cm^{-2}, (c) $F=270$ μJ cm^{-2}, (d) $F=130$ μJ cm^{-2}, and (e) $F=67$ μJ cm^{-2}. In the inset the dependence of τ_{HM} on the fluence is shown in a double logarithmic plot together with linear fit with a slope of -0.45. The pump photon energy was $E_{pump}=E_g+1$ eV.

increasing fluence the rise times decrease and also the delay τ at which the rise takes place decreases. From the inset of Fig. 8 one can recognize that the correlation between τ_{HM} and the fluence can be written within good approximation in the form

$$\tau_{HM} \propto 1/F^{0.45}.$$

F. Summary of experimental results

After the applicability of the differential reflection technique with probing the soh-c transition as a TOF method was shown, a series of experiments with varying the sample thickness d were performed at a fluence of $F=800$ μJ cm^{-2}. Relatively sharp charge-carrier fronts were observed with arrival times τ_{HM}, which correlate with the thickness d as $d \propto \tau_{HM}^{0.33}$. High initial carrier velocities of $v(\tau=10\,\text{ps})=14\times10^5$ cm/s decrease within 500 ps to values in the range of $v(\tau=400\,\text{ps})=2\times10^5$ cm/s. From the TOF measurements with variable E_{pump} at constant pulse energies we conclude that the observed plasma expansion is rather insensitive to the initial kinetic energy of the carriers. The fluence of the pump pulses was found to be the dominating parameter, controlling the expansion velocity of the plasma. At a fixed thickness d the correlation between the arrival time τ_{HM} and the fluence F can be described by $\tau_{HM} \propto 1/F^{0.45}$.

These experimental facts lead to the question about the underlying driving force of the observed fast carrier transport. In the next section this question will be discussed within a simple hydrodynamic model.

V. MODEL

Diffusive carrier transport in the hydrodynamic limit is described with thermodynamic variables in a local thermodynamic equilibrium.[19] We neglect all effects due to hot carriers and hot phonons and assume constant quasitemperatures of the electrons and holes of $T=300$ K. In an optically generated plasma an equal density of electrons and holes was generated. The long-range Coulomb potentials of the carriers prohibit significant charge separation (Dember effect), so that electrons and holes move together in a plasma cloud. In this ambipolar transport only one carrier density $n(n_e=n_h\equiv n)$ needs to be considered, which satisfies the ambipolar diffusion equation[19]

$$\frac{\partial n}{\partial t}=\nabla[D(n)\cdot\nabla n]+G+R \tag{1}$$

with the local carrier density n, the generation rate G, and the recombination rate R. All nonlinearities are condensed in the charge-carrier-dependent diffusivity $D(n)$. Note that $\nabla[D(n)\cdot\nabla n]\neq D(n)\Delta n$, because of the density dependence of the diffusivity D. Because the short temporal width of our pump pulses ($\sim$100 fs) compared to the time scale of the observed transport, the pulse duration can be neglected within good approximation in our simulations. Only nonlinear recombination is taken into account,

$$R=-Bn^2-Cn^3, \tag{2}$$

with the Auger recombination coefficient $C=7\times10^{-30}\,\text{cm}^6\,\text{s}^{-1}$ and the bimolecular recombination coefficient $B=1.7\times10^{-10}\,\text{cm}^3\,\text{s}^{-1}$ following Ref. 20. The linear recombination via impurity recombination, which would lead to a term of $-An$ in Eq. (2), strongly depends on the purity of the observed sample and therefore would need to be measured independently. Because of the large recombination times $\tau>1$ ns this recombination process can be neglected.

As the main effect resulting in a density-dependent diffusivity, we consider the so-called *Fermi pressure*. It originates from the fact that for sufficiently high densities, i.e., with the onset of degeneracy, Pauli's exclusion principle needs to be considered and the free energy is significantly higher than it would be in a classical gas. The enhancement of free energy Φ depends on the carrier density n and therefore on the volume V. This can be interpreted as a pressure: $p=\partial\Phi/\partial V$. A quantitative description[19] starts with the dependence of the local carrier densities $n_c(c=e,h)$ on the quasi-Fermi-levels ψ_c resulting from the integration of the Fermi distribution functions $f_c(\mathbf{r},\mathbf{p})$ over momentum space,

$$n_c=2\left[\frac{m_c\beta}{2\pi\hbar^2}\right]^{3/2}\mathcal{F}_{1/2}(\beta\psi_c), \tag{3}$$

with $\beta=1/(kT)$, the effective masses m_c, and $\mathcal{F}_n$ the nth-order Fermi integral:

$$\mathcal{F}_n(z)=\frac{1}{\Gamma(n+1)}\int_0^\infty\frac{x^n}{\exp(x-z)+1}dx. \tag{4}$$

The quasi-Fermi-levels ψ_c are measured relatively to their respective band edges.

These considerations lead to an ambipolar diffusivity D, depending on the quasi-Fermi-levels[5,19]

$$D=\frac{1}{nq\beta}\frac{\sigma_e\sigma_h}{\sigma_e+\sigma_h}\left(\frac{\mathcal{F}_{1/2}(\beta\psi_e)}{\mathcal{F}_{-1/2}(\beta\psi_e)}+\frac{\mathcal{F}_{1/2}(\beta\psi_h)}{\mathcal{F}_{-1/2}(\beta\psi_h)}\right) \tag{5}$$

with the absolute value of the electrical conductivity of the elctrons/holes σ_c given by

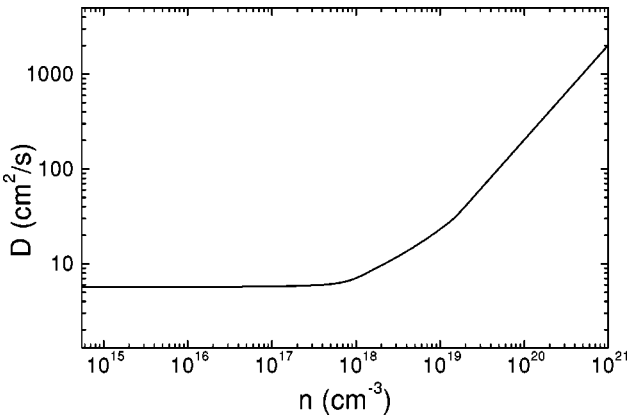

FIG. 9. Density-dependent diffusivity resulting from the Fermi pressure with the low-density diffusion constants $D_e^0 = 100\ \mathrm{cm^2\ s^{-1}}; D_h^0 = 3\ \mathrm{cm^2 s^{-1}}$.

$$\sigma_c = e n_c \mu_c^0 \frac{\mathcal{F}_0(\beta\psi_c)}{\mathcal{F}_{1/2}(\beta\psi_c)}, \tag{6}$$

where μ_c^0 is the mobility of the charge carriers in a Maxwell-Boltzmann distribution and e the elementary charge.

In the low-density limit ($\beta_c\psi_c \ll 1$), where $\mathcal{F}_i/\mathcal{F}_j = 1$, Eqs. (5) and (6) lead to the known ambipolar diffusion constant that satisfies the Einstein relation. In the degenerate case ($\beta_c\psi_c \gg 1$) the Einstein relation loses its validity. In this high-density limit the Fermi integrals can be solved and lead to[5]

$$\psi_c = \frac{\hbar^2 (3\pi^2 n_c)^{2/3}}{2 m_c}, \tag{7}$$

$$\frac{\mathcal{F}_0(\beta\psi_c)}{\mathcal{F}_{1/2}(\beta\psi_c)} = \frac{3\sqrt{\pi}}{4}(\beta\psi_c)^{-1/2}, \quad \frac{\mathcal{F}_{1/2}(\beta\psi_c)}{\mathcal{F}_{-1/2}(\beta\psi_c)} = \frac{2}{3}\beta\psi_c . \tag{8}$$

Equation (6) describes the reduction of the mobility of the carriers due to the fact that for the degenerate case only carriers beneath the Fermi surface contribute to the transport. This means that at high densities the conductivity rises only with $\sigma \propto n^{2/3}$ instead of $\sigma \propto n$ in the nondegenerate case. The driving force of the Fermi pressure results in the $\mathcal{F}_{1/2}/\mathcal{F}_{-1/2}$ terms of Eq. (5), which are proportional to $n^{2/3}$ at sufficiently high densities.

For the description of our experiment however, the complete function $D(n)$ in the density range $0 \leqslant n \leqslant n_{max}$, with the maximum density of generated carriers n_{max}, is needed. Therefore the integrals in Eq. (5) were solved numerically and the resulting $\mathcal{F}_i(n)/\mathcal{F}_j(n)$ were fitted with suitable functions, so that the low- and high-density limits were fulfilled and the transition between them is comparable with the calculations. The resulting $D(n)$ curve is plotted in Fig. 9. It can be seen that D remains nearly constant until about $n \sim 10^{18}\ \mathrm{cm^{-3}}$, where the degeneracy of the electron system at $T = 300$ K sets in. At $n \sim 2 \times 10^{19}\ \mathrm{cm^{-3}}$, the transition of the hole system from the nondegenerate to the degenerate case takes place. At higher densities the diffusivity is nearly proportional to n.

With $D(n)$ from Fig. 9, Eq. (1) was solved numerically, where the diffusivity at each site i for time step j was set to $D(n_i^{j-1})$. Only the one-dimensional transport perpendicular to the surface was taken into account, because in our experiment the sample thickness $d \leqslant 2.5$ μm was much smaller than the focus diameter of the pump beam of 20 μm. The carrier profile at $\tau = 0$ was set to $n(\tau = 0, z) \propto \exp[-\alpha_{pump} z]$. For simplicity the surfaces were set to be totally reflecting for the carriers.[21] For comparison of the simulated $n(\tau, z)$ with the experimental data, the $\Delta R_{trans}(\tau)$ signal was assumed to be proportional to the carrier density $n = n(z = d)$.

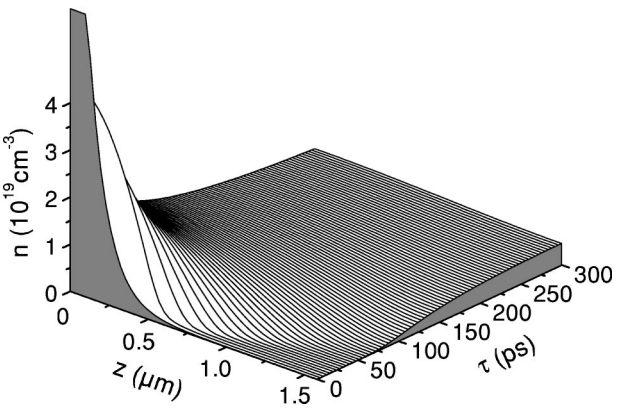

FIG. 10. Three-dimensional plot of the simulated time- and space-dependent carrier distribution function. Initial carrier density $n_0 = 1.6 \times 10^{20}\ \mathrm{cm^{-3}}$. Sample thickness $d = 1.6$ μm.

VI. DISCUSSION

A. Numerical results

In Fig. 10 the simulated spatiotemporal dynamics of the charge-carrier density $n(z, \tau)$ is shown. The carriers initially generated near $z = 0$ relax within about 300 ps via carrier-density-dependent diffusion towards a spatially homogeneous distribution function. After this time the overall carrier density decreases due to the carrier recombination. Fast diffusing carriers within the high-density plasma that are held back by the slowly diffusing carriers at the leading edge of the plasma cloud lead to the formation of a relatively sharp carrier front that travels through the sample. The fast decrease of the carrier density at $z = 0$ results not only from the fast transport of the carriers but also from the fast plasma and Auger recombination at high densities [see Eq. (2)].

B. Comparison of the simulation with experiment

The results of our model are now compared with the experimental data. In Fig. 11 the experimental $\Delta R_{trans}(\tau)$ curves are shown together with the calculated data for different sample thicknesses d. It can be seen that the calculated signals describe fairly well the observed delay and thickness dependence of the measured $\Delta R_{trans}(\tau)$ curves. From the inset it can be seen that the theory yields a correlation between the thickness d and the delay at half of the maximum signal of the form τ_{HM} of

$$d \propto \tau_{HM}^{0.36},$$

which is comparable with the experimentally found correlation of $d \propto \tau_{HM}^{0.33}$. Also the faster decreasing times for smaller

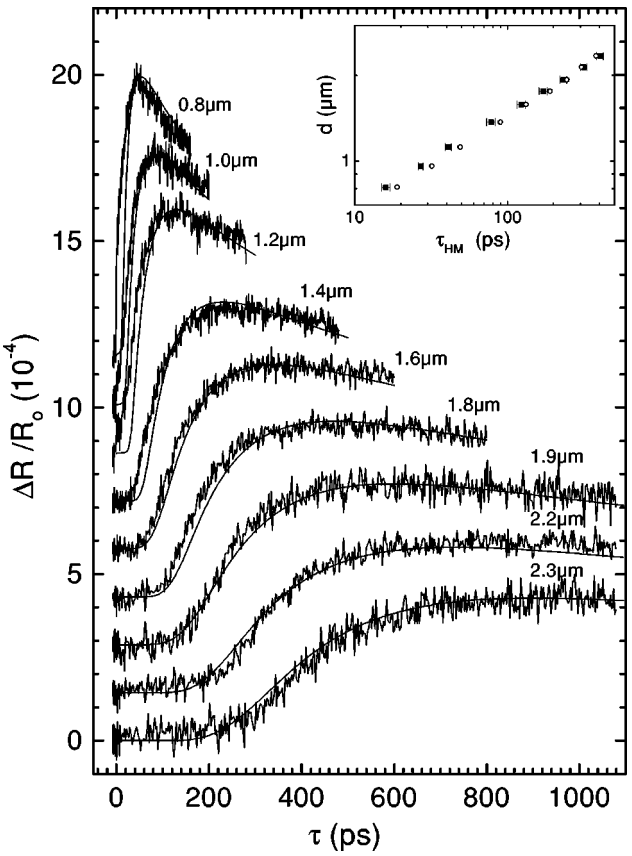

FIG. 11. Variation of the sample thickness: Comparison of the theory with the experiment at a pump fluence of $F=800\,\mu\mathrm{J\,cm^{-2}}$, which corresponds to a initial carrier density of $n=1.2\times10^{20}\,\mathrm{cm^{-3}}$. In the inset the correlation between the sample thickness d and the arrival time τ_{HM} of the carriers in a double logarithmic scale is shown (solid squares, experiment; open circles, theory).

sample thicknesses d arising from the density-dependent carrier recombination are qualitatively reproduced with the model.

In Fig. 12 the theoretical and experimental curves of $\Delta R_{trans}(\tau)$ for increasing fluence of the pump pulses are shown. All theoretical curves were simulated with the same

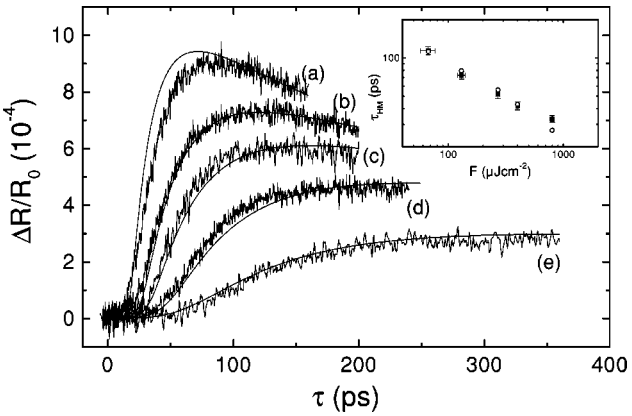

FIG. 12. Variation of the pump fluence: Comparison of the theory with the experiment at a sample thickness of $d=1.0\ \mu$m. In the inset the dependence of the arrival times τ_{HM} on the pump fluence in a double logarithmic scale is shown (solid squares, experiment; open circles, theory).

set of parameters as in Fig. 11 but only changing the initial carrier density and the sample thickness. Here also the model fairly well describes the main characteristics of the experimental observations. The simulated arrival times of the carriers τ_{HM} depending on the fluence F are in agreement with experiment within the experimental error except for the highest fluence of $F=800\,\mu\mathrm{Jcm^{-2}}$ (see inset of Fig. 12). In a double logarithmic plot the theoretical data points of $\tau_{HM}(F)$ can be fitted with a line of slope -0.56, which is comparable with the experimentally found slope of -0.45.

The good agreement of the model with the experimental results lead to the conclusion that the Fermi pressure is the underlying driving force for the observed plasma expansion. Poles *et al.*[5] also interpreted their time-resolved luminescence studies on GaAs epilayers of different thicknesses with a fast plasma transport originating from the Fermi pressure.

C. Discussion of other effects influencing the plasma transport

At high carrier densities also the renormalization of the self-energies of the carriers due to many-body effects needs to be considered. In the simplest approximation, only the change of the band gap E_g depending on the total carrier density n is considered with a formula given in Ref. 22. Such a band gap shrinkage would lead to an additional term in the diffusion equation,[19] which *reduces* the diffusivity:

$$\frac{\partial n}{\partial t}=G+R+\nabla\cdot\left\{D(n)\nabla n\left[1+n\beta\times\left(\frac{\mathcal{F}_{1/2}(\beta\psi_e)}{\mathcal{F}_{-1/2}(\beta\psi_e)}+\frac{\mathcal{F}_{1/2}(\beta\psi_h)}{\mathcal{F}_{-1/2}(\beta\psi_h)}\right)\frac{\partial E_g}{\partial n}\right]\right\}. \qquad (9)$$

Numerical calculations of Eq. (9) show that the band gap renormalization would lead to a reduction of the total diffusing constant D including the Fermi pressure with increasing n and for densities $n>10^{19}\,\mathrm{cm^{-3}}$ to a negative diffusivity and hence a carrier confinement. This, however, is not observed in our experiment. This discrepancy could result from the fact that the diffusivity is affected by carriers at the Fermi wave vector $\boldsymbol{k}_f$ and not at $k\approx0$. A more detailed many-body theory[23] shows that the energy reduction extends in k space only to one or two times $\boldsymbol{k}_f$. Therefore the influence of the self-energy correction is overestimated in Eq. (9). However, the measured longer arrival time in comparison with the theory at the highest fluence in Fig. 12 could be effected by the self-energy renormalization effect.

Another effect influencing the plasma transport is the screening of the carrier–LO-phonon scattering,[1] which is the dominating momentum scattering process at room temperature determing the diffusivity of charge carriers in GaAs.[24] As a first approximation this effect could be taken into account with density-dependent mobilities $\mu_c=\mu_c(n)$. Calculations that take this effect into account with scattering times taken from Ref. 25 show that this effect leads to a further increase of the ambipolar diffusivity. This increase, however, is small compared to increase of diffusivity resulting from the Fermi pressure.

As already mentioned, all effects resulting from the generation of hot carriers had to be neglected in our model, but they could influence the plasma transport. Monte Carlo simulation studies[26] predict that within the cooling times of the

carriers a fast transport of the carriers takes place. The influence of the initial carrier temperature on the plasma transport could not be observed within our experiments (see Sec. IV D). In our experiment the direct measured velocities are not found to be limited by the velocity of sound $v_{sound}^{GaAs} \approx 5 \times 10^5$ cm/s. This fact leads to the conclusion that for our experimental conditions the so-called phonon wind is not the dominating driving force.

For the lateral transport the possibility of plasma transport via emission and reabsorption of photons is discussed in the literature.[3,4,8,10] Gao *et al.*[11] also explained their results of supersonic velocities of the plasma expansion perpendicular to the surface, deduced from the duration of longitudinal acoustic pulses, with this photon recycling process. Because the transport due to the photon recycling process depends not on the density gradient,[8] and therefore it should not be describable with a diffusion equation. In contrast to this, our results can be reasonably well described by a model based on a diffusion equation. This fact leads to the conclusion that the photon recycling process does not seems to be the dominating process responsible for the observed plasma expansion.

VII. SUMMARY

With the measurement of the differential reflection (ΔR) and differential transmission (ΔT) for either co-and counterpropagating pump and probe geometries as a function of the time delay τ and the sample thickness d a novel time-of-flight method for the investigation of charge-carrier transport perpendicular to the surface is presented. We take advantage of the fact that ΔR, in contrast to ΔT, is only sensitive to carriers near the reflecting surface. This method enables a direct observation of the spatiotemporal dynamics of charge-carrier plasmas for time delays $\tau \ll 100$ ps. The spatial resolution that lies in the range of about half the absorption length of the probe pulses has been enhanced with probing the transition from the spin-orbit-split hole (soh) band in GaAs to the conduction band to ~ 0.17 μm.

With this method investigations of carrier-density-dependent plasma transport in the direct semiconductor GaAs at room temperature were performed with fluences $60\ \mu\mathrm{J\ cm^{-2}} \leqslant F \leqslant 800\ \mu\mathrm{J\ cm^{-2}}$. At a pump fluence of $F = 800\ \mu\mathrm{J\ cm^{-2}}$ initially high expansion velocities of about 14×10^5 cm/s at $\tau \approx 20$ ps were observed that decrease to about 2×10^5 cm/s at $\tau \approx 350$ ps. The correlation between the sample thickness d and the arrival times τ_{HM} of the carriers was found to be $d \propto \tau_{HM}^{0.33}$. The plasma transport shows a strong dependence on the pump fluence. At a fixed sample thickness d the arrival times of the plasma τ_{HM} depend on the fluence F as $\tau_{HM} \propto 1/F^{0.45}$.

Numerical simulations with a density-dependent diffusivity D, which show a qualitatively good agreement with the experimental data, lead to the conclusion that for the chosen geometry and experimental parameters the Fermi pressure is the dominating driving force for the plasma transport. The formation of a relatively sharp carrier front can be understood by fast diffusing carriers within the high-density plasma that are held back by the slowly diffusing carriers at the leading edge of the plasma cloud.

[1] For a review see J. Shah, *Ultrafast Spectroscopy of Semiconductors and Semiconductor Nanostructures*, Springer Series in Solid State Sciences Vol. 115 (Springer, Berlin, 1996).

[2] F.M. Sterenka and J.P. Wolfe, Phys. Rev. Lett. **53**, 2181 (1984).

[3] H. Hillmer, S. Hansmann, and A. Forchel, Phys. Rev. B **45**, 8782 (1992), and references therein.

[4] R. Cingolani, K. Ploog, A. Cingolani, C. Moro, and M. Ferrara, Phys. Rev. B **42**, 2893 (1990); **45**, 8785 (1992).

[5] E. Poles, D. Huppert, M.C. Hanna, and Y. Rosenwaks, J. Appl. Phys. **86**, 3481 (1999); E. Poles, S.Y. Goldberg, B. Fainberg, D. Huppert, M.C. Hanna, and Y. Rosenwaks, *ibid.* **80**, 5129 (1996).

[6] H. Nakata, A. Uddin, and E. Otsuka, Semicond. Sci. Technol. **7**, 1266 (1992).

[7] K.T. Tsen, O.F. Sankey, G. Halama, S.-C.Y. Tsen, and H. Marcoc, Phys. Rev. B **39**, 6276 (1989); K.T. Tsen, G. Halama, O.F. Sankey, S.-C.Y. Tsen, and H. Marcoc, *ibid.* **40**, 8103 (1989).

[8] E.C. Fox and H.M. van Driel, Phys. Rev. B **47**, 1663 (1993).

[9] M. Petrauskas, S. Juodkazis, V. Netikis, M. Willander, A. Ouacha, and B. Hammerlund, Semicond. Sci. Technol. **7**, 1355 (1992).

[10] I.J. Blewett, N.R. Gallaher, A.K. Kar, and B.S. Wherrett, J. Opt. Soc. Am. B **13**, 779 (1996).

[11] W. Gao, V. Gusev, C. Glorieux, J. Thoen, and G. Borghs, Opt. Commun. **143**, 19 (1997).

[12] H. Hillmer, A. Forchel, T. Kuhn, G. Mahler, and H.P. Maier, Phys. Rev. B **43**, 13 992 (1991); G. Mahler, T. Kuhn, A. Forchel, and H. Hillmer, in *Optical Nonlinearities and Instabilities in Semiconductors*, edited by H. Haug (Academic Press, Boston 1988), Chap. 7.

[13] H.W. Yoon, D.R. Wake, J.P. Wolfe, and H. Markoc, Phys. Rev. B **46**, 13 461 (1992).

[14] L.M. Smith, J.S. Preston, J.P. Wolfe, D.R. Wake, J. Klem, T. Henderson, and H. Markoc, Phys. Rev. B **39**, 1862 (1989).

[15] C.V. Shank, D.H. Auston, E.P. Ippen, and O. Teschke, Solid State Commun. **26**, 567 (1978).

[16] G. Böhne, S. Freund, S. Lehmann, and R.G. Ulbrich, in *Proceedings of the 7th International Symposium on Ultrafast Processes in Spectroscopy Bayreuth, 1991*, edited by A. Laubereau and A. Seilmeier, IOP Conf. Proc. No. 126 (IOP, London, 1992), p. 329.

[17] D.E. Aspnes, and A.A. Studna, Phys. Rev. B **27**, 985 (1983).

[18] A. Alexandrou, V. Berger, and D. Hulin, Phys. Rev. B **52**, 4654 (1995).

[19] H.M. van Driel, Phys. Rev. B **35**, 8166 (1987).

[20] U. Strauss and W.W. Rühle, Appl. Phys. Lett. **62**, 55 (1993).

[21] The influence of the boundary conditions, especially the surface recombination velocity is discussed in by Kuhn *et al.* (Ref. 12). We included in our simulations a surface recombination velocity as a variable parameter and found that it does not significantly alter the density dependence of the plasma transport.

[22] P. Vashishta and R.K. Kalia, Phys. Rev. B **25**, 6492 (1982).

[23] R. Blank and H. Haug, Phys. Rev. B **44**, 10 513 (1991).

[24] See, for instance, K. Seeger, *Semiconductor Physics* (Springer, Wien, 1973).

[25] S. Das Sarma, J.K. Jain, and R. Jalabert, Solid-State Electron. **31**, 695 (1988).

[26] R.P. Joshi, K.T. Tsen, and D.K. Ferry, Phys. Rev. B **41**, 9899 (1990).